

Assembling a lasing hybrid material with supramolecular polymers and nanocrystals

LEIMING LI¹, ELIA BENIASH¹, EUGENE R. ZUBAREV², WANGHUA XIANG³, BRYAN M. RABATIC², GUIZHONG ZHANG³ AND SAMUEL I. STUPP^{*1,2,4}

¹Department of Materials Science and Engineering, ²Department of Chemistry and ⁴Feinberg School of Medicine, Northwestern University, Evanston, Illinois 60208, USA

³College of Precision Instruments and Optoelectronics Engineering, Tianjin University, Tianjin 300072, China

*e-mail: s-stupp@northwestern.edu

Published online: 21 September 2003; doi:10.1038/nmat983

The combination of bottom-up and top-down processes to organize nanophases in hybrid materials is a key strategy to create functional materials. We found that oxide and sulphide nanocrystals become spontaneously dispersed in organic media during the self-assembly of nanoribbon supramolecular polymers. These nanoribbon polymers form by self-assembly of dendron rodcoil molecules, which contain three molecular blocks with dendritic, rod-like, and coil-like architectures. In an electric field these supramolecular assemblies carrying bound nanocrystals migrate to the positive electrode in an etched channel and align in the field. In the system containing ZnO nanocrystals as the inorganic component, both phases are oriented in the hybrid material forming an ultraviolet lasing medium with a lower threshold relative to pure ZnO nanocrystals.

Over the past decade great progress has been made on synthesis of nanostructures as a tool-set for new materials and nanotechnology. Inorganic examples include semiconductor quantum dots^{1–3}, carbon nanotubes⁴, inorganic nanowires^{5,6}, nanobelts⁷ and metal clusters^{8,9}. Organic structures with dimensions in the nanometre range have also been prepared shaped as tubes¹⁰, mushrooms¹¹, ribbons¹², fibres¹³ and dendritic particles^{14,15}. The organization of very large arrays of nanostructures into functional systems that go well beyond the nanoscale has been a less-common topic of research. The systems reported include colloidal crystals of quantum dots², piezoelectric layered films of mushroom-shaped objects¹⁶, carbon nanotube single crystals¹⁷ and nanowire arrays⁶. We report here on the dispersion of inorganic nanocrystals of ZnO, TiO₂ and CdS from the bottom of organic solutions during the self-assembly of monomers into ribbon-shaped supramolecular polymers. We also report on properties of millimetre-size arrays of these hybrid dispersions aligned in electric fields.

Dilute solutions in organic solvents of dendron rodcoil (DRC) molecules, with blocked covalent architecture consisting of coil-like, rod-like and dendritic segments, were previously reported to self-assemble into nanoribbons (see Fig. 1). These nanoribbons have widths of 10 nm, thickness of 2 nm, and lengths of up to 10 μ m (ref. 12). In this work, we mixed ZnO nanocrystals (average particle size of 24–71 nm, purchased from Nanophase Technologies, Illinois) in dilute solutions of DRC molecules in 2-ethylhexyl methacrylate (EHMA). The ZnO size range was confirmed by transmission electron microscopy (TEM), and most of the crystals were found to be single crystals as revealed by electron diffraction. In a typical experiment, 20 mg of DRC molecules and 20 mg of ZnO nanocrystals were added to 1 g of EHMA solvent, and the mixture was ultrasonicated and then heated in an 80 °C water bath. Interestingly, without disturbance at room temperature, the ZnO crystals become dispersed throughout the organic medium as self-assembly proceeds. As a control sample, an isotropic aqueous poly(vinyl alcohol) (PVA) gel was also prepared by adding 20 mg of PVA (purchased from Aldrich, M_w : 124,000 to 186,000) and 20 mg of the same ZnO crystals in 1 g of water. The solution was stirred and ultrasonicated for 30 minutes. About 0.13 g of saturated borax water

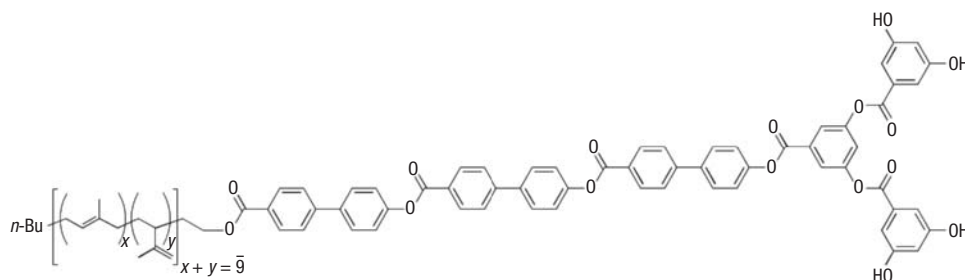


Figure 1 Chemical structure of a dendron rodcoil (DRC) molecule.

solution (at room temperature) was then added to promote gelation in the solution¹⁸ while it was stirred and sonicated for another 30 minutes. Without disturbance the PVA gel was formed in about one week.

Figure 2a shows the ZnO dispersed in DRC gel and its corresponding mineral concentration profile—measured using reflection-mode photoluminescence—as a function of height. In Fig. 2b, the concentration profile of ZnO in the PVA gel demonstrates that most of the mineral has remained at the bottom of the vial. We succeeded in achieving similar dispersions for CdS crystals (Fig. 2c; average particle size of ~50 nm) as well as TiO₂ crystals (not shown; average particle size of 25–51 nm, Nanophase Technologies.). All images in Fig. 2 were taken at least one month after the gels were formed.

Without any ultrasonication (just heating to 80 °C) but otherwise following the same procedures described above, we prepared another DRC gel and a PVA gel both containing ZnO crystals, and kept them undisturbed for over 6 months. In this case, a more remarkable difference was observed in dispersion of crystals between the self-assembling DRC gel and the isotropic PVA gel. In the PVA sample, the gel appears transparent whereas there is very obvious opacity in the DRC gel due to dispersion of ZnO crystals. Therefore, self-assembly of the nanoribbon supramolecular polymers results in much more effective dispersion of ZnO crystals relative to a crosslinked gel of an ordinary polymer. As no ultrasonication was applied, some large clusters of ZnO crystals remain at the bottom of the DRC gel.

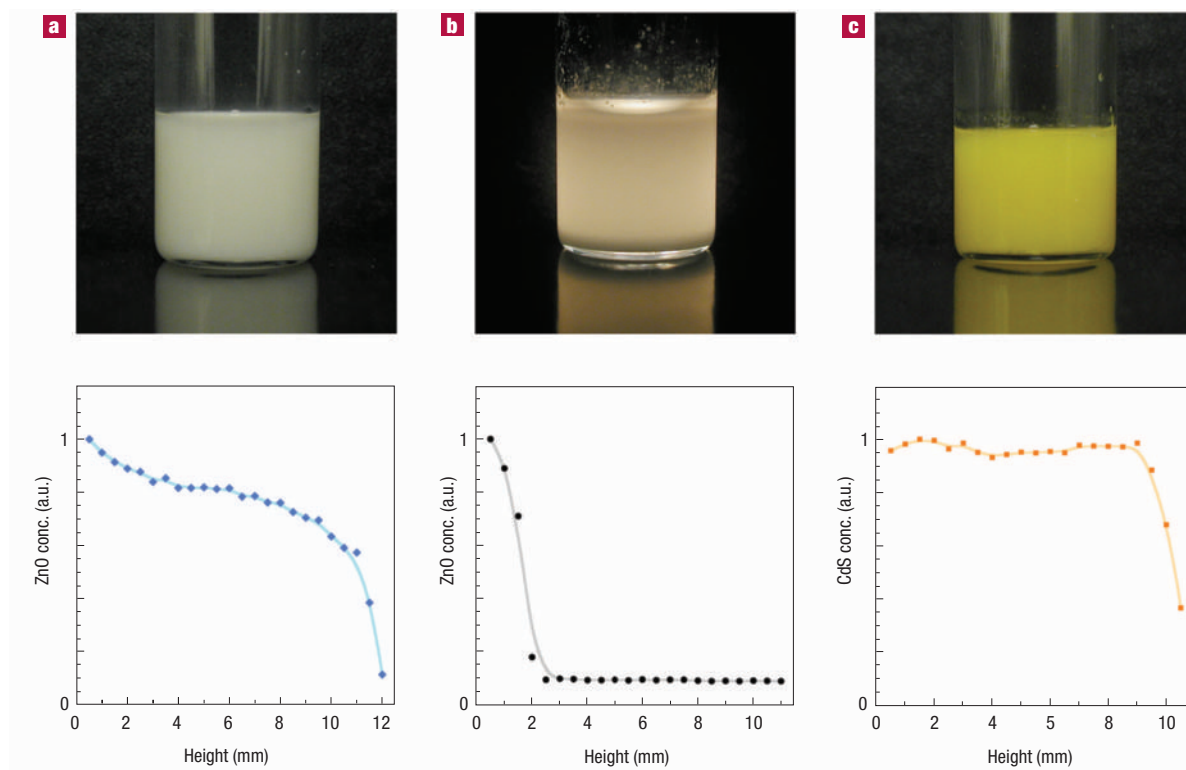


Figure 2 Strong dispersion of nanocrystals in DRC gels. **a**, Photograph of a 2 wt% ZnO–2 wt% DRC–EHMA gel and its vertical concentration profile for ZnO nanoparticles. **b**, photograph of a 2 wt% ZnO–2 wt% PVA–H₂O gel and its vertical concentration profile for ZnO nanoparticles. **c**, Photograph of a 2 wt% CdS–2 wt% DRC–EHMA gel and its vertical concentration profile for CdS nanoparticles. The gel in **b** was illuminated from behind to reveal the ZnO sediment, and all photographs were taken at least one month after gelation.

In Fig. 3 we show a schematic representation of crystal dispersion as organic nanoribbons form by self-assembly. We are not certain at this time what might be the mechanism of crystal dispersion during this self-assembly process. However, it is possible that binding and therefore dispersion of crystals by the rigid 10-nm-wide polymers is much more effective than binding and dispersion by flexible and thin polymer chains. One would expect DRC nanoribbons and PVA chains to have similar capacity to bind crystals based on OH group functionality. OH groups are of course present in repeats of PVA and on the basis of earlier structural studies of the nanoribbons¹² we expect free OH (phenolic) groups to be present in DRC nanoribbons as well. However, the greater rigidity and surface area per monomer in DRC nanoribbons (widths equivalent to tens of ordinary polymer chains) could make them more effective binders of crystals. This way, crystals trapped by the nanoribbons are effectively dispersed against gravity by Brownian motion.

The high aspect ratio of the nanoribbons offers the possibility of uniaxial alignment in electric fields. In addition, ZnO crystals have a polar c axis¹⁹, and therefore once bound to nanoribbons could be simultaneously aligned by the field in hybrid materials. For this purpose, a glass coated with indium tin oxide (ITO) was etched using hydrochloric acid to form two rectangular ITO electrodes leaving a gap with a width between 0.3 and 2 mm where gels were placed and exposed to electric fields. Before applying the field, both DRC–EHMA and ZnO–DRC–EHMA gels appeared birefringent with randomly oriented domains when viewed optically between crossed polarizers (P and A; see Fig. 4a). On application of a d.c. electric field of $\sim 1,500 \text{ V cm}^{-1}$ or higher, a clear liquid (which later proved to be EHMA monomer) oozed out of

the gel towards the negative electrode side. At the same time, strongly birefringent domains moved slowly towards the positive electrode. These observations suggest the occurrence of electrophoresis²⁰ separating the DRC nanoribbons from the solvent of the gel. Poling for one day resulted in a visually smooth film with a thickness between 10 and $20 \mu\text{m}$ as measured by a surface profiler (Tencor, P-10). The net weight of the poled film was about 4% that of the 2 wt%DRC–2 wt%ZnO–EHMA gel placed in the etched gap before poling, or about 2% when a 2 wt% DRC–EHMA gel was poled. We therefore conclude that most of the EHMA monomer evaporated during poling, leaving a solid material formed by nanoribbons that migrated to the positive electrode.

In Fig. 4b, a poled DRC film is shown in which the poling direction makes a 45° angle with the directions of the polarizer and analyzer in the microscope. When the poled film was rotated so that the poling direction was parallel or perpendicular to the polarizer–analyzer pair (shown in Fig. 4c), the transmitted light intensity was greatly reduced. Thus, Fig. 4b,c suggests a unidirectional orientation of DRC nanoribbons in the poled film²¹. Similar unidirectional birefringence was observed in DRC–ZnO poled samples. We also analysed ultramicrotomed sections of the poled DRC film by TEM. The TEM image in Fig. 5a from the samples sectioned along the poling direction shows nanoribbons with a spacing of about 8–9 nm that are parallel to the poling direction. No nanoribbons could be observed in samples sectioned perpendicular to the poling field (see Fig. 5b). The TEM and polarized microscopy indicate that nanoribbons align mostly parallel to the poling direction and collapse into unidirectional dense arrays. This destroys the nanoribbon network that exists in the gel state before

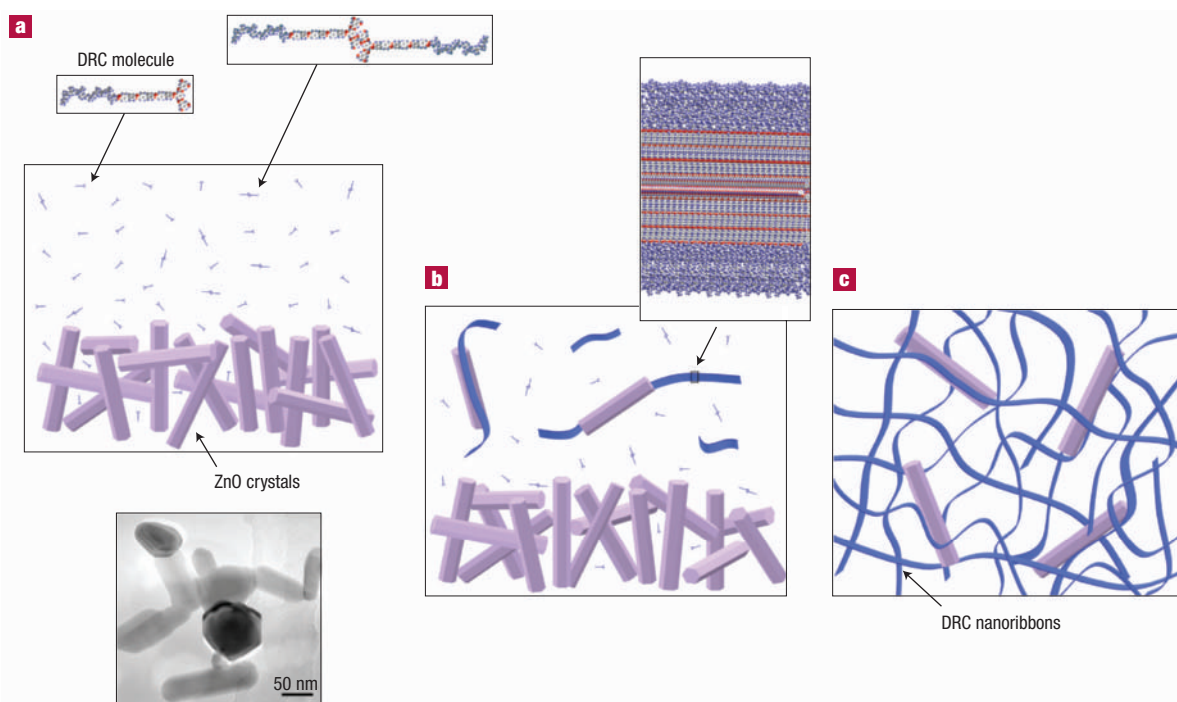


Figure 3 Schematic representation of ZnO nanocrystal dispersion from the bottom of organic solutions by nanoribbons formed by self-assembly of DRC molecules. **a**, Crystals are at the bottom of the monomer solution before self-assembly of DRC molecules; also shown is a TEM image of some typical ZnO crystals. The darker areas in the image correspond to the ZnO crystals aligned normal to the figure plane. **b**, Crystals are bound by nanoribbons as self-assembly proceeds. **c**, The network of nanoribbons with bound and dispersed crystals.

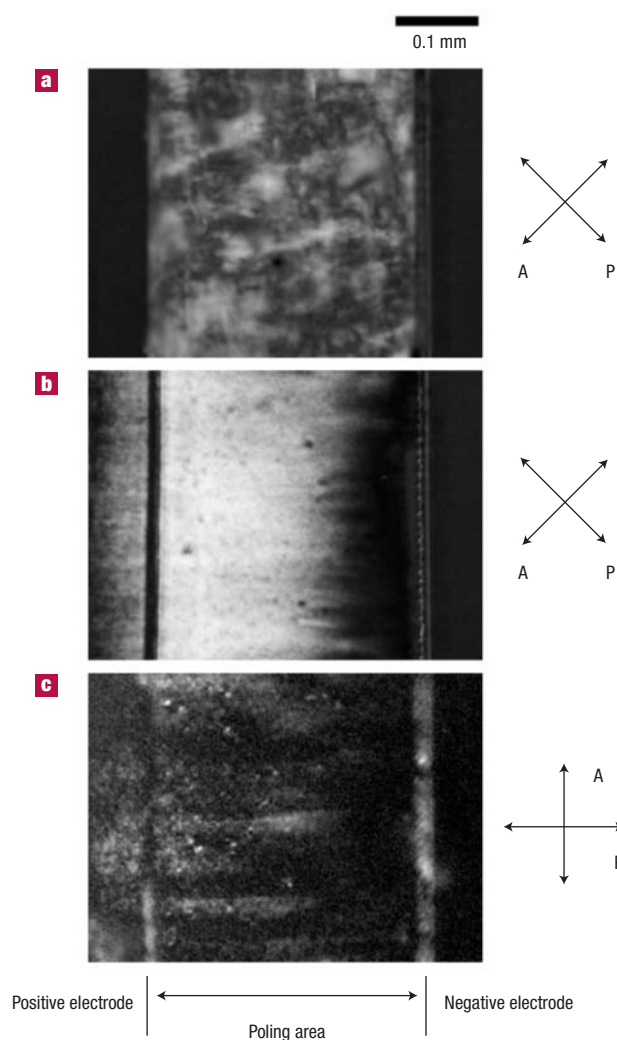


Figure 4 Electric fields unidirectionally orient DRC nanoribbons. **a,b**, Optical micrographs between crossed polarizers (A and P) of a 2 wt% DRC–EHMA before **(a)** and after **(b)** exposure to a $1,500 \text{ V cm}^{-1}$ electric field. **c**, Optical micrograph obtained when the poling field direction is parallel to P and perpendicular to A.

solvent evaporation. We believe that the migration of ribbons to the positive electrode could be based on partial ionization of phenolic groups, and that inter-ribbon hydrogen bonding could be an important stabilization factor in the collapsed gel.

Electrical orientation of the ZnO crystals during electrophoresis was investigated using ultraviolet–visible spectroscopy and second-harmonic generation (SHG) measurements. A Cary 500 UV-VIS spectrophotometer was used to obtain absorption spectra of the poled DRC–ZnO thin films using linearly polarized light and scanning through the intrinsic absorption wavelengths²² of ZnO. When the sample was placed with the poling direction parallel to the electric field E of the light, its absorption spectrum showed a consistent blue shift of $30 \pm 5 \text{ meV}$ relative to the spectrum obtained with E perpendicular to the poling direction (see Fig. 6). The shift, which should be due to ZnO intrinsic exciton absorption selection rules at room temperature, indicates that the ZnO crystals have a preferential c -axis orientation along the poling direction^{23,24}. As the similarly poled pure DRC

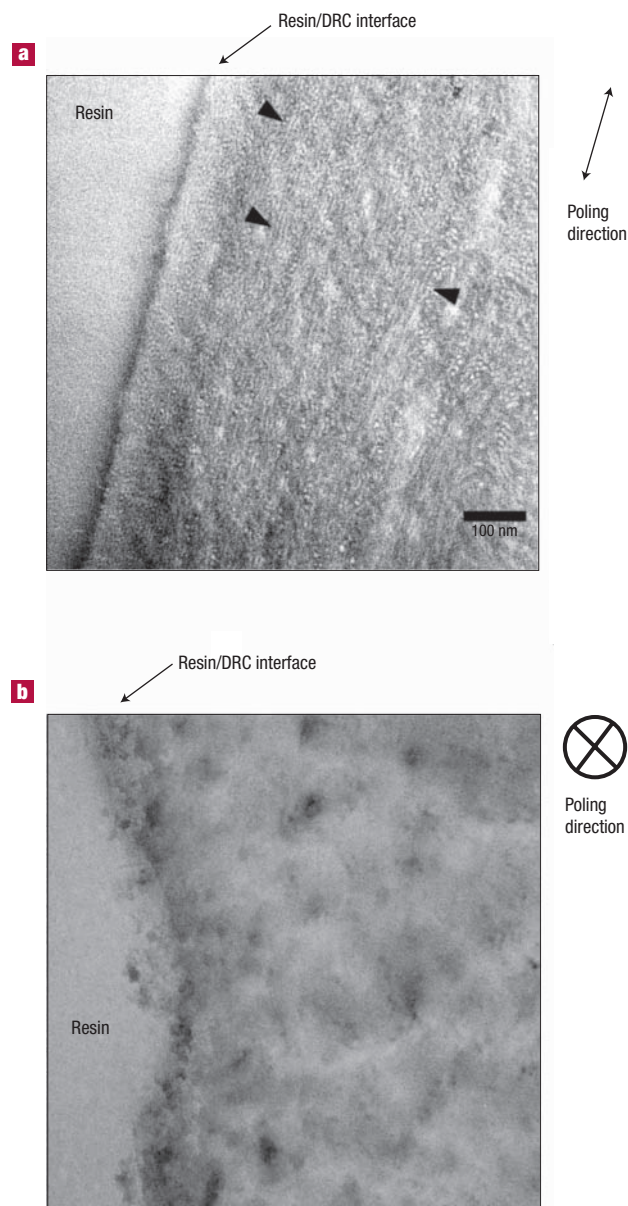


Figure 5 TEM reveals the orientation of DRC nanoribbons along the poling direction. **a,b**, TEM micrographs of the OsO_4 -stained poled DRC nanoribbon film sectioned parallel **(a)** and perpendicular **(b)** to the poling direction. The black arrowheads in **a** point to some of the nanoribbons in the micrograph.

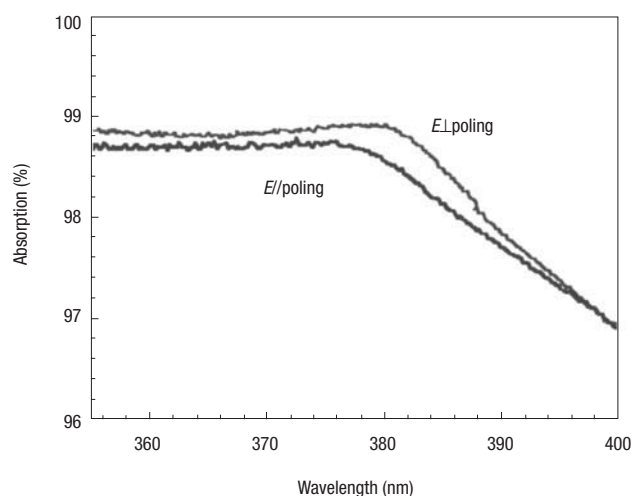
nanoribbon film did not show this difference, we attribute the shift to ZnO orientation. The preferential c -axis orientation is also consistent with the fact that polar ZnO single crystals would align along the applied electric field to lower their energy²⁵. Annealing at 100°C for one day did not change the absorption shift significantly, suggesting the structural stability of the poled DRC–ZnO film at this temperature. SHG measurements also suggested that the ZnO crystals in the poled DRC nanoribbons orient with field direction. It was found that the p-polarized SHG signals produced with either s- or p-polarized fundamental beams were significantly larger than the s-polarized SHG

Table 1 Second harmonic generation (SHG) signals produced with either s- or p-polarized fundamental light from poled ZnO–DRC films.

Fundamental polarization	p	s	s	p
SHG polarization	p	p	s	s
I_{SHG} (a.u.)	663 ± 56	591 ± 15	392 ± 15	398 ± 23

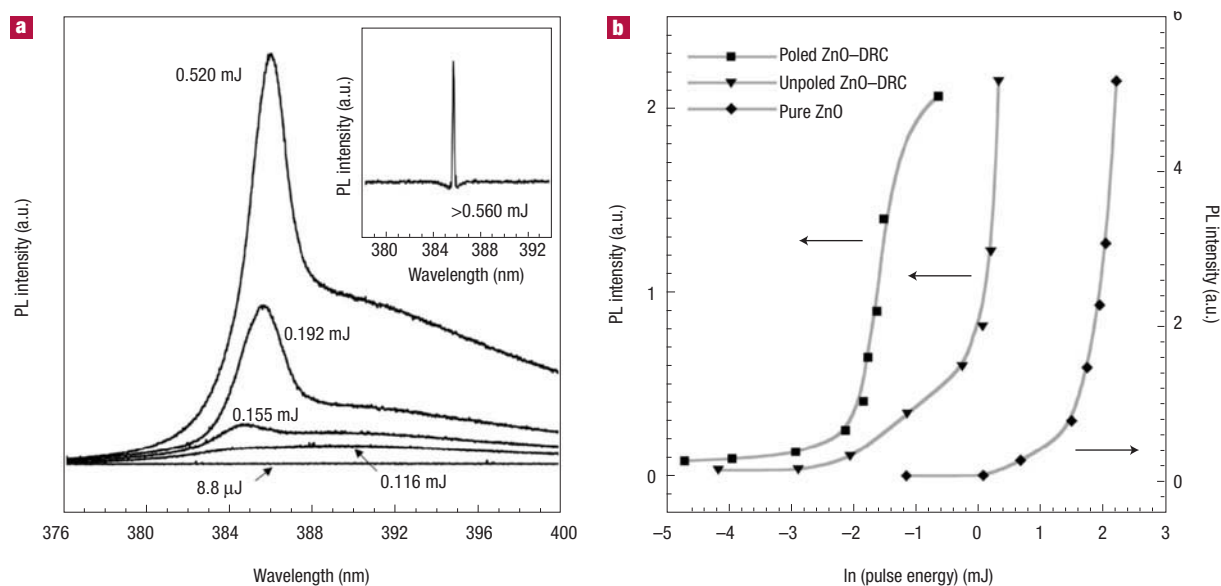
signals (see Table 1). As the poling direction of films is parallel to the electric field of the p-polarized incident beam, this anisotropic distribution of SHG intensity again suggests a preferential *c*-axis orientation of the ZnO nanocrystals.

Ultraviolet emission from ZnO has attracted great interest in recent years^{6,26–31} and we therefore measured this property in the aligned hybrid materials. At room temperature, ZnO has a direct bandgap in the ultraviolet range (3.37 eV) and an exciton binding energy of 60 meV, making it a potential candidate for room-temperature-operated ultraviolet light-emitting diodes (LEDs) and lasers³⁰. The embedded ZnO nanocrystals in the poled DRC films (generated from the 2 wt%ZnO–2 wt%DRC–EHMA gel) gave rise to ultraviolet emission at room temperature when excited with a Q-switched mode-locked Nd:YAG laser (355 nm, 10 Hz, 35 ps). When the pumping laser power was gradually increased, broad spontaneous emissions were first observed, followed by peak sharpening and faster growth rates of emission intensity as pumping exceeded a threshold value (shown representatively in Fig. 7a). The peak intensity (in arbitrary units) versus the natural logarithm of pumping laser single pulse energy is plotted in Fig. 7b revealing clearly a threshold behaviour. When pulse energy exceeded ~ 0.560 mJ, peaks in the spectra were extremely narrow

**Figure 6** Ultraviolet–visible absorption spectra of poled ZnO–DRC hybrid films with the electric field of the linearly polarized probe light either parallel (E//poling) or perpendicular (E⊥poling) to the poling direction.

with a full-width at half-maximum of 0.18 ± 0.03 nm (Fig. 7a, inset) and $\sim 100\%$ polarized.

We also prepared control samples by firmly sandwiching between two glass slides a thin layer (defined by spacers 25 μm thick) of the same ZnO crystals used in the other experiments. When subjected to the same pumping setup, lasing emissions did occur from these samples, but interestingly the threshold (measured in single pulse energy) was 40 ± 7 times higher than that of the poled DRC–ZnO film (Fig. 7b). We also measured the threshold for identically prepared but unpoled

**Figure 7** Ultraviolet emission from poled DRC–ZnO films with lower threshold. **a**, Increasing pumping power induces emission peak growth and narrowing from ZnO nanocrystals in the poled DRC–ZnO film (pumping pulse energy is indicated for each spectrum). Extremely sharp spectra occur for a pulse energy over ~ 0.560 mJ (inset). **b**, Representative curves of photoluminescence (PL) peak intensity versus \ln of pumping laser pulse energy for the poled ZnO–DRC film, unpoled ZnO–DRC film, and the pure ZnO powder control sample that has a nanocrystal density about twice that in the poled and unpoled ZnO–DRC films.

DRC–ZnO films. The threshold (in single pulse energy) ratio of the pure ZnO crystals to the unpoled DRC–ZnO samples was 6.7 ± 3.8 (Fig. 7b). Even though the exact mechanism for the decreasing threshold values remains unknown, one could suggest that it may be related to the macroscopic orientation of ZnO crystals guided by nanoribbon arrays. ZnO powder samples are not expected to have any significant macroscopic orientation of crystals. ZnO media with a high degree of structural order such as ZnO nanowire arrays⁶ or epilayers grown on lattice-matched substrates^{28,29} tend to have a lower lasing threshold than those with a low degree of order such as non-epitaxial ZnO films^{32,33}, or ZnO pellets made of pressed powders³⁴. In this context it may be reasonable to suggest that the much lower threshold relative to control samples is connected to the higher order parameter achieved in the poled DRC–ZnO hybrid material by combining nanoscale self-assembly and crystal dispersion with externally applied potentials. In unpoled DRC–ZnO films, DRC nanoribbons form domains with sizes around 0.1 mm that match the diameter of the focused pumping laser beam. Within each domain the nanoribbons have a preferred orientation, thus aligning the elongated ZnO rods to some degree as well. This may lower the threshold for lasing relative to pure ZnO powder samples. In conjunction with top-down methods for patterning, such orienting processes may be useful in the preparation of photonically active microscopic structures.

METHODS

REFLECTION-MODE PHOTOLUMINESCENCE

A 355 nm Nd:YAG laser (Continuum, YG 601) was used for the photoluminescence experiments. An aperture limited the laser beam diameter to ~0.5 mm. The gel was scanned with the laser from the bottom to the top of the glass vial in 0.5 mm steps. Photoluminescence was measured in reflection mode from the ZnO or CdS particles dispersed in the gel. The mineral particle concentration was assumed to be proportional to the integrated photoluminescence intensity.

TEM OF ULTRAMICROTOMED SAMPLES

The poled DRC nanoribbon film was pre-stained with a 2% aqueous solution of OsO₄ for two hours, and then frozen and lyophilized. The film was placed in EMBED 812 embedding medium (Electron Microscopy Sciences) that was polymerized at 70 °C. The ultrathin sections of the DRC film parallel and perpendicular to the poling direction were cut on an ultramicrotome device (MT600, RMC). The sections were then mounted on copper TEM grids, post-stained in OsO₄ vapour, and studied with a Hitachi 8100 HR TEM at an accelerating voltage of 200 kV.

SECOND-HARMONIC GENERATION

A Q-switched Nd:YAG laser (Quanta Ray, DCR-1) (1,064 nm, 10 Hz, 5 ns), either p- or s-polarized, was used for the SHG experiments. The focused 1,064-nm fundamental beam was incident normal to the poled DRC–ZnO film, whose poling direction was chosen to be parallel to the electric field of the p-polarized incident laser. The second harmonic at 532 nm generated from the ZnO nanocrystals was separated from the fundamental by an infrared filter and a monochromator. The light was collected in a photomultiplier tube, and the signal was recorded with a digital data acquisition system (SRS Boxcar, SR280). A polarizer was placed right after the sample to selectively pass the p- or s-component of the SHG signals generated.

Received 30 December 2002; accepted 22 August 2003; published 21 September 2003.

References

- Bawendi, M. G., Steigerwald, M. L. & Brus, L. E. The quantum mechanics of larger semiconductor clusters ("quantum dots"). *Annu. Rev. Phys. Chem.* **41**, 477–496 (1990).
- Murray, C. B., Kagan, C. R. & Bawendi, M. G. Self-organization of CdSe nanocrystallites into three-dimensional quantum dot superlattices. *Science* **270**, 1335–1338 (1995).
- Alivisatos, A. P. Semiconductor clusters, nanocrystals, and quantum dots. *Science* **271**, 933–937 (1996).
- Iijima, S. Helical microtubules of graphitic carbon. *Nature* **354**, 56–58 (1991).

- Duan, X., Huang, Y., Cui, Y., Wang, J. & Lieber, C. M. Indium phosphide nanowires as building blocks for nanoscale electronic and optoelectronic devices. *Nature* **409**, 66–69 (2001).
- Huang, M. H. *et al.* Room-temperature ultraviolet nanowire nanolasers. *Science* **292**, 1897–1899 (2001).
- Pan, Z. W., Dai, Z. R. & Wang, Z. L. Nanobelts of semiconducting oxides. *Science* **291**, 1947–1949 (2001).
- Mirkin, C. A., Letsinger, R. L., Mucic, R. C. & Storhoff, J. J. A DNA-based method for rationally assembling nanoparticles into macroscopic materials. *Nature* **382**, 607–609 (1996).
- Alivisatos, A. P. *et al.* Organization of 'nanocrystal molecules' using DNA. *Nature* **382**, 609–611 (1996).
- Ghadiri, M. R., Granja, J. R., Milligan, R. A., McRee, D. E. & Khazanovich, N. Self-assembling organic nanotubes based on a cyclic peptide architecture. *Nature* **366**, 324–327 (1993).
- Stupp, S. I. *et al.* Supramolecular materials: self-organized nanostructures. *Science* **276**, 384–389 (1997).
- Zubarev, E. R., Pralle, M. U., Sone, E. D. & Stupp, S. I. Self-assembly of dendron rodcoil molecules into nanoribbons. *J. Am. Chem. Soc.* **123**, 4105–4106 (2001).
- Harterink, J. D., Beniash, E. & Stupp, S. I. Self-assembly and mineralization of peptide-amphiphile nanofibers. *Science* **294**, 1684–1688 (2001).
- Leon, J. W., Kawa, M. & Fréchet, J. M. J. Isophthalate ester-terminated dendrimers: versatile nanoscopic building blocks with readily modifiable surface functionalities. *J. Am. Chem. Soc.* **118**, 8847–8859 (1996).
- Hudson, S. D. *et al.* Direct visualization of individual cylindrical and spherical supramolecular dendrimers. *Science* **278**, 449–452 (1997).
- Pralle, M. U. *et al.* Piezoelectricity in polar supramolecular materials. *Angew. Chem. Int. Edn* **39**, 1486–1489 (2000).
- Schlittler, R. R. *et al.* Single crystals of single-walled carbon nanotubes formed by self-assembly. *Science* **292**, 1136–1139 (2001).
- Casassa, E. Z., Sarquis, A. M. & Van Dyke, C. H. The gelation of polyvinyl alcohol with borax. *J. Chem. Edu.* **63**, 57–60 (1986).
- Van De Pol, F. C. M. Thin-film ZnO - properties and applications. *Am. Ceram. Soc. Bull.* **69**, 1959–1965 (1990).
- Hawcroft, D. M. *Electrophoresis The Basics* (Oxford Univ. Press, Oxford, 1997).
- Hecht, E. & Zajac, A. *Optics* (Addison-Wesley, Massachusetts, 1974).
- Sasanuma, M. Optical processes in ZnO. *J. Phys. Condens. Matter* **7**, 10029–10036 (1995).
- Gorla, C. R. *et al.* Structural, optical, and surface acoustic wave properties of epitaxial ZnO films grown on (0112) sapphire by metalorganic chemical vapor deposition. *J. Appl. Phys.* **85**, 2595–2602 (1999).
- Liang, W. Y. & Yoffe, A. D. Transmission spectra of ZnO single crystals. *Phys. Rev. Lett.* **20**, 59–62 (1968).
- Keller, F. J., Gettys, W. E. & Skove, M. J. *Physics Classical and Modern* 2nd edn (McGraw-Hill, New York, 1993).
- Cao, H., Xu, J. Y., Seelig, E. W. & Chang, R. P. H. Microlaser made of disordered media. *Appl. Phys. Lett.* **76**, 2997–2999 (2000).
- Sun, Y., Ketterson, J. B. & Wong, G. K. L. Excitonic gain and stimulated ultraviolet emission in nanocrystalline zinc-oxide powder. *Appl. Phys. Lett.* **77**, 2322–2324 (2000).
- Kawasaki, M. *et al.* Excitonic ultraviolet laser emission at room temperature from naturally made cavity in ZnO nanocrystal thin films. *Mater. Sci. Eng. B* **56**, 239–245 (1998).
- Chen, Y., Bagnall, D. & Yao, T. ZnO as a novel photonic material for the UV region. *Mater. Sci. Eng. B* **75**, 190–198 (2000).
- Look, D. C. Recent advances in ZnO materials and devices. *Mater. Sci. Eng. B* **80**, 383–387 (2001).
- Thareja, R. K. & Mitra, A. Random laser action in ZnO. *Appl. Phys. B* **71**, 181–184 (2000).
- Mitra, A. *et al.* Synthesis and characterization of ZnO thin films for UV laser. *Appl. Surf. Sci.* **174**, 232–239 (2001).
- Cho, S. *et al.* Photoluminescence and ultraviolet lasing of polycrystalline ZnO thin films prepared by the oxidation of the metallic Zn. *Appl. Phys. Lett.* **75**, 2761–2763 (1999).
- Mitra, A. & Thareja, R. K. Photoluminescence and ultraviolet laser emission from nanocrystalline ZnO thin films. *J. Appl. Phys.* **89**, 2025–2028 (2001).

Acknowledgements

This paper is based on work supported by the US Department of Energy (DE-FG02-00ER45810) and the US Army Research Office (DAAG55-97-1-0126). Any opinions, findings, and conclusions or recommendations expressed in this publication are those of the authors and do not necessarily reflect the views of the Department of Energy or the Army Research Office. Correspondence and requests for materials should be addressed to S.I.S.

Competing financial interests

The authors declare that they have no competing financial interests.